PERGAMON

Chemical Engineering Science 58 (2003) 4173–4184

Chemical Engineering Science

www.elsevier.com/locate/ces

Dynamic behavior and sensitivity of skeleton thermokinetic model for acetaldehyde oxidation

C. H. Liang[a], C. Y. Mou[a], D. J. Lee[b,*]

[a] *Department of Chemistry, National Taiwan University, Taipei 10617, Taiwan*
[b] *Department of Chemical Engineering, National Taiwan University, Taipei 10617, Taiwan*

Received 29 November 2002; received in revised form 16 May 2003; accepted 2 June 2003

Abstract

This work elucidated the dynamic behavior of the Wang–Mou model, a three-variable, skeleton model for acetaldehyde oxidation, in a continuously stirred tank reactor. The characteristics of the five dynamic regimes reported in the literature were numerically explored herein, specifically: (I) low-temperature steady state, (II) oscillatory two-stage ignitions, (III) complex oscillations, (IV) oscillatory cool flames, and (V) high-temperature steady state. Regimes were noted with new dynamic characteristics, which had not previously been reported. Additionally, bifurcations around the bistable and the birhythmic regimes were examined in detail.

The sensitivity analysis polynomial approximation method revealed the significance of the kinetic parameters on the system's dynamics. Furthermore, the sequences of the sensitivity coefficients for the five dynamic regimes were reported. The step which initiates oxidation controls the ignition oscillation's dynamics, while the low-temperature branching and high-temperature termination steps control the cool flame.

Keywords: Acetaldehyde oxidation; Continuous stirred tank reactor; Oscillation; Bifurcation

1. Introduction

The chemical reaction for equimolar mixtures of acetaldehyde and oxygen in a continuous-flow stirred tank (CSTR) can generate various dynamic behaviors, including steady states, bistability, cool-flame oscillations, ignition oscillation, and complex ignition-cool flame oscillations (Gray, Griffiths, Hasko, & Lignola, 1981a, b). Detailed chemical analyses have been conducted to interpret these experimental findings (Halstead, Prothero, & Ouinn, 1971; Felton, Gray, & Shank, 1976; Gibson, Gray, Griffiths, & Hasko, 1984; Kaiser, Westbrook, & Pitz, 1986; Pugh, De Kock, & Ross, 1986; Harrison & Cairnie, 1988; Griffiths & Sykes, 1989; Cavangh, Cox, & Olson, 1990; Di Maio, Lignola, & Talarico, 1993). For instance, the model proposed by Felton et al. (1976) could describe the cool-flame oscillation phenomena. Additionally, the 25 elementary reactions proposed by Gibson et al. (1984) can be used to generate the complex ignition oscillation sequence. However, these analyses fail to provide a theoretical framework for the in-depth understanding of the above-mentioned complex dynamic behavior for acetaldehyde oxidation system.

The detailed kinetic scheme for hydrocarbon oxidation comprises numerous elementary reactions whose importance varies with temperature and pressure and involve autocatalytic chain-branching mechanisms. Yang and Gray (1969) developed a two-variable (the autocatalytic chain carrier and the pool temperature) skeleton model as follows:

$$Y \rightarrow X \quad \text{initiation,} \tag{1a}$$

$$X \rightarrow 2X \quad \text{low-temperature branching,} \tag{1b}$$

$$X \rightarrow S_1 \quad \text{high-temperature termination,} \tag{1c}$$

$$X \rightarrow S_2 \quad \text{low-temperature termination,} \tag{1d}$$

where Y represents the fuel and oxygen (both concentration assumed equal) and X is the autocatalytic chain carrier. Assuming a constant concentration of reactant y and the following sequence for activation energies, $E_{1c} > E_{1b} > E_{1d}$,

* Corresponding author. Fax: +886-2-2362-5632.
E-mail address: djlee@ccms.ntu.edu.tw (D. J. Lee).

0009-2509/$ - see front matter © 2003 Elsevier Ltd. All rights reserved.
doi:10.1016/S0009-2509(03)00300-2

the steady states and the cool-flame oscillations (located in the regime of negative temperature effect) were successfully simulated.

The Gray–Yang model cannot generate the complex ignition oscillation patterns observed experimentally (Gray et al., 1981a, b) and in simulation works depend on detailed kinetics (Gibson et al., 1984). This shortcoming is attributed mainly to the fact that the Gray–Yang model has just two variables, insufficient to describe a complex dynamic system that requires at least three degrees of freedom. Wang and Mou (1985) refined the Gray–Yang model by considering fuel consumption and adding a high temperature branching step. Furthermore, Wang and Mou used their novel model to reproduce the five distinct dynamic states observed experimentally (Eq. (3a)–(3c)), namely: (I) low-temperature steady state, (II) oscillatory two-stage ignitions, (III) complex oscillations (IV) oscillatory cool flames, and (V) high-temperature steady state. Wang and Mou also presented the bifurcation diagram for these states and, in doing so, demonstrated the complex sequence noted in regime III. Furthermore, as addressed in Wang and Mou, numerous questions remain unanswered in connection with the dynamic behavior, particularly the details of how and why the states transit between distinct regimes, and the sensitivity of the model parameters for the dynamic behavior. Scott (1991) and Griffiths (1995) comprehensively reviewed the literature on skeleton kinetic models.

This study numerically investigates the Wang–Mou model. The rest of this paper is organized as follows. Section 2 briefly summarizes the Wang–Mou model. Section 3 then describes the numerical simulations of the Wang–Mou model, and discusses the dynamic characteristics of the five regimes on both the $P - T_0$ and $\tau - T_0$ state diagrams. The method of state transit among different regimes is examined. Simulations were conducted to investigate new dynamic states. In Section 4, sensitivity analysis of parameters in the Wang–Mou model is conducted using the polynomial approximation method (PAM). Significant parameters in the five dynamic states are identified individually. Conclusions are finally made in Section 5.

2. The Wang–Mou model

The Wang–Mou model can be displayed as follows:

$$Y \xrightarrow{k_1} X \quad \text{initiation,} \tag{2a}$$

$$X + Y \xrightarrow{k_2} 2X \quad \text{high-temperature branching,} \tag{2b}$$

$$X \xrightarrow{k_3} 2X \quad \text{low-temperature branching,} \tag{2c}$$

$$X \xrightarrow{k_1} S_1 \quad \text{high-temperature termination,} \tag{2d}$$

$$X \xrightarrow{k_5} S_2 \quad \text{low-temperature termination.} \tag{2e}$$

The rate constants, k_i's, take Arrhenius forms, whose activation energy E_i's follow $E_2 > E_1 > E_4 > E_3 > E_5$. Further assume that the reactor is perfectly mixed (CSTR) with residence time of $\tau = 1/k_f$, in which case adopting the Newtonian cooling obtains the following mass and energy balance equations:

$$\frac{\mathrm{d}\bar{x}}{\mathrm{d}\bar{t}} = \bar{k}_1\bar{y} + \bar{k}_2\overline{xy} - (\bar{k}_5 + \bar{k}_4 - \bar{k}_3)\bar{x} - k_f\bar{x}, \tag{3a}$$

$$\frac{\mathrm{d}\bar{y}}{\mathrm{d}\bar{t}} = -\bar{k}_1\bar{y} - \bar{k}_2\overline{xy} - k_f(\bar{y} - y_0), \tag{3b}$$

$$C\frac{\mathrm{d}\bar{T}}{\mathrm{d}\bar{t}} = \bar{k}_1\bar{h}_1\bar{y} + (\bar{k}_2\bar{h}_2\bar{y} + \bar{k}_3\bar{h}_3 + \bar{k}_4\bar{h}_4 + \bar{k}_5\bar{h}_5) \times\bar{x} - \bar{k}_T(\bar{T} - T_0), \tag{3c}$$

where $\bar{x}$ and $\bar{y}$ are the concentrations of X and Y, $\bar{T}$ is the temperature of the CSTR, $\overline{h_i}$'s are the heat of reaction, and C is the specific heat of the system. Then, the introduction of the following dimensionless groups into Eqs. (3a)–(3c) leads to the governing equations: $x = \bar{x}/y_0$; $y = \bar{y}/y_0$; $U = (\bar{T} - T_0)/T_0$; $t = k_f\bar{t}$; $k_2 = \bar{k}_2 y_0/k_f$; $k_j = \bar{k}_j/k_f (j \neq 2)$; $h_j = \bar{h}_j y_0/T_0 C$; $k_T = \bar{k}_T/Ck_f$:

$$\frac{\mathrm{d}x}{\mathrm{d}t} = k_1 y + k_2 xy - (k_5 + k_4 - k_3)x - x, \tag{4a}$$

$$\frac{\mathrm{d}y}{\mathrm{d}t} = -k_1 y - k_2 xy + 1 - y, \tag{4b}$$

$$\frac{\mathrm{d}U}{\mathrm{d}t} = k_1 h_1 y + (k_2 h_2 y + k_3 h_3 + k_4 h_4 + k_5 h_5)x - k_T x. \tag{4c}$$

Notably, let $k_2 = 0$ then Eqs. (4a)–(4c) can be reduced to the original Gray–Yang model.

Table 1 lists the thermokinetic parameters adopted to solve Eqs. (4a)–(4c), which are identical to those adopted in Wang and Mou.

Table 1
Thermokinetic parameters in Wang–Mou model

$\bar{k}_1(\mathrm{s}^{-1}) = A_1 N_0 \exp(-E_1/RT)$	$A_1 = 1.6 \times 10^{10}$	$E_1 = 24$ kcal mol^{-1}	$\bar{h}_1 = 0$ kcal mol^{-1}
$\bar{k}_1(\mathrm{mol}^{-1}\ \mathrm{cm}^3\ \mathrm{s}^{-1}) = A_2 \exp(-E_1/RT)$	$A_2 = 7.4 \times 10^{12}$	$E_2 = 25$ kcal mol^{-1}	$\bar{h}_2 = 92$ kcal mol^{-1}
$\bar{k}_3(\mathrm{s}^{-1}) = A_3 N_0 \exp(-E_3/RT)$	$A_3 = 1.38 \times 10^8$	$E_3 = 7$ kcal mol^{-1}	$\bar{h}_3 = 4$ kcal mol^{-1}
$\bar{k}_4(\mathrm{s}^{-1}) = A_4 N_0 \exp(-E_4/RT)$	$A_4 = 7.8 \times 10^{10}$	$E_4 = 16$ kcal mol^{-1}	$\bar{h}_4 = 20$ kcal mol^{-1}
$\bar{k}_5(\mathrm{s}^{-1}) = A_5 N_0^{1/2}/d$	$A_5 = 3.3 \times 10^3$	$E_5 = 0$ kcal mol^{-1}	$\bar{h}_5 = 0$ kcal mol^{-1}
$\bar{k}_T(\mathrm{calc\ m}^{-3}\mathrm{K}^{-1}\mathrm{s}^{-1}) = 3.68 \times 10^{-1}$			

$\bar{k}_j = \bar{k}_{j0}\exp(-E_j/RT) = \bar{k}_{j0}\exp(-1/\varepsilon_j)\exp(U/\varepsilon_j(1+U)), \varepsilon_j = RT_0/E_j.$

3. Bifurcation diagrams

3.1. $P - T_0$ diagram

3.1.1. Regimes I–V

As a slice out of a three-dimensional picture, with τ as the third dimension, Fig. 1 illustrates the bifurcation diagram for the Wang–Mou model in the $P - T_0$ space at $\tau = 4$ s. Five distinct dynamic behavior regimes were noted. Regime I presents stable node dynamics (low-temperature steady state), while Regime V displays a stable focus (high-temperature steady state). Relaxation oscillations occur in Regime II, corresponding to the two-stage ignition, while oscillatory cool flames appear in Regime IV. Regime III exhibits characteristics that combine those of Regimes II and IV. Wang and Mou illustrated the phase portraits for Regimes II–IV.

According to the bifurcation diagram presented in Fig. 1, an isobar at $P = 67.9$–85.3 kPa represents a horizontal line crossing Regimes I–V. Fig. 2 displays the bifurcation sequence of Regimes II–IV at $P = 73.6333$ kPa. P_1^m is denoted herein as the case with one large-amplitude oscillation and m small-amplitude oscillations per period. With an increment of T_0 of 0.01 K, an odd-m sequence ($m = 1, 3, 5, \ldots$) is observed to proceed from left to right; while some sequences with even-m ($m = 2, 4, 6, \ldots$) move from right to left. Fig. 3 displays an example at T_0 that changes from 578.08 K (P_1^5) to 578.00 K (P_1^3). The observation for P_1^m bifurcation correlates with Wang and Mou (1985). Reducing the increments of T_0 (10^{-4} K) causes chaotic sequences. $C_1^{m,n}$ is denoted as the case with one large-amplitude oscillation and mixed m and n small-amplitude oscillations per period. Fig. 4 shows the sequence of complex oscillations at two distinct residence times. Chaos occurs among P_1^m oscillations. Gaspard and Wang (1987) and Wang and Gaspard (1990) also demonstrated complex oscillations using Wang–Mou model.

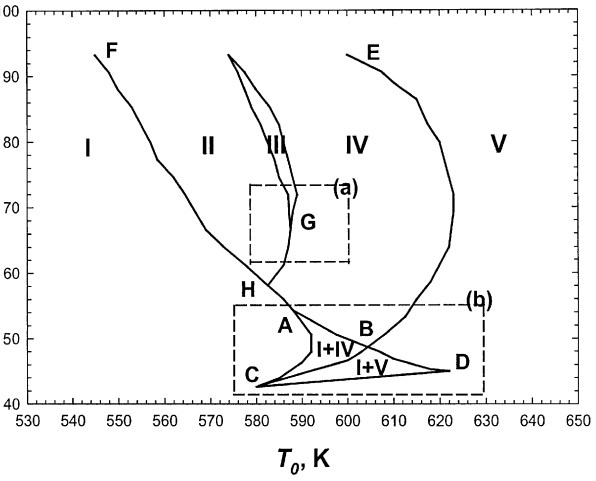

Fig. 1. The $P-T_0$ bifurcation diagram for acetaldehyde oxidation predicted by Wang–Mou model. $\tau = 4$ s.

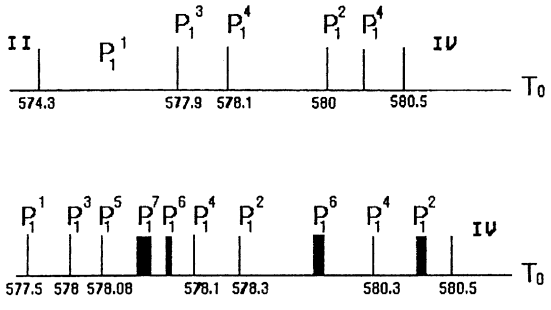

Fig. 2. Complex oscillation sequences in Regime III. $P = 73.6333$ kPa, $\tau = 10$ s. Between states P_1^m and P_1^{m+2} are complex oscillations $C_1^{m,m+2}$.

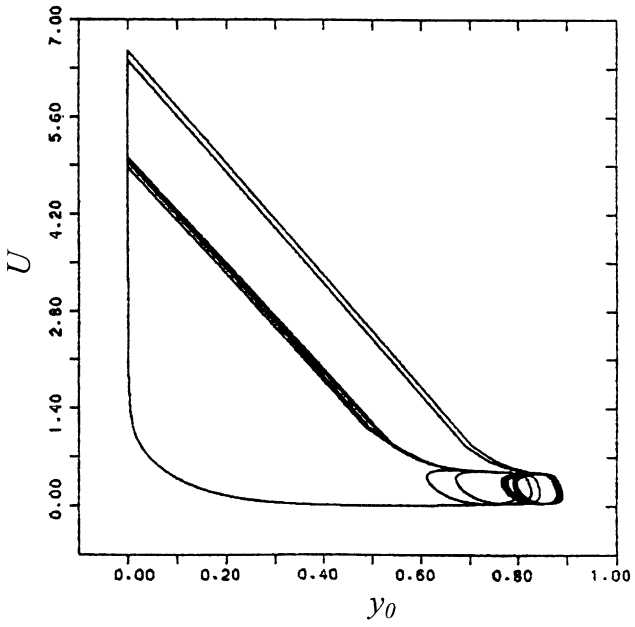

Fig. 3. Phase portrait of chaotic state of $C_1^{3,5}$. $P = 73.6333$ kPa, $T_0 = 589.4255$ K, $\tau = 4$ s.

According to Fig. 1 Regime III exists in an intermediate region, above and below which Regimes II and IV merge. Wang and Mou suggested that a direct transition between Regimes II and IV can be achieved without crossing Regime III. Fig. 5 illustrates an example of direct transitions between Regimes II and IV by changing T_0.

Besides the five regimes described above, a birhythmic regime (a narrow region of width less than 0.5 K along curve GH) and two bistable regimes (I+IV and I+V) were noted. Significantly, the existence of the birhythmicity in Wang–Mou model is identified for the first time, and the locations of the bistable regimes differ from those illustrated in Wang and Mou (1985). The bifurcation characteristics around the birhythmicity regime (enveloped region (a) in Fig. 1) and around the bistable regimes (enveloped region (b) in Fig. 1) are discussed in detail.

(a)

P=73.6333 kPa, τ=4 s.

Sequence	$\rightarrow P_1^1 \rightarrow$	$\rightarrow C_1^{1,3} \rightarrow$	$\rightarrow P_1^3 \rightarrow$	$\rightarrow C_1^{3,5} \rightarrow$	$\rightarrow P_1^5 \rightarrow$	$\rightarrow C_1^{5,7} \rightarrow$	$\rightarrow P_1^7 \rightarrow$	$\rightarrow C_1^{7,9} \rightarrow$	$\rightarrow P_1^9 \rightarrow$	$\rightarrow \rightarrow$
T_0 (K)	589.285	589.289	589.4	589.4255	589.451	589.4514	589.4515	589.4557	589.456	

	$\rightarrow P_1^8 \rightarrow$	$\rightarrow C_1^{6,8} \rightarrow$	$\rightarrow P_1^6 \rightarrow$	$\rightarrow C_1^{4,6} \rightarrow$	$\rightarrow P_1^4 \rightarrow$	$\rightarrow C_1^{4,2} \rightarrow$	$\rightarrow P_1^2 \rightarrow$
	589.458	589.459	589.46	589.4723	589.55	589.615	589.62

(b)

P=73.6333 kPa, τ=10 s.

Sequence	$\rightarrow P_1^1 \rightarrow$	$\rightarrow C_1^{1,3} \rightarrow$	$\rightarrow P_1^3 \rightarrow$	$\rightarrow C_1^{3,5} \rightarrow$	$\rightarrow P_1^5 \rightarrow$	$\rightarrow C_1^{5,7} \rightarrow \rightarrow$	$\rightarrow C_1^{6,4} \rightarrow$	$\rightarrow P_1^4 \rightarrow$	$\rightarrow C_1^{2,4} \rightarrow$	$\rightarrow P_1^2 \rightarrow$
T_0 (K)	577.5	577.83	578	578.05	578.08	578.0905	578.093	578.1	578.2	578.3

Fig. 4. Bifurcation sequence in Regime III. $P = 73.6333$ kPa, $\tau = 10$ s.

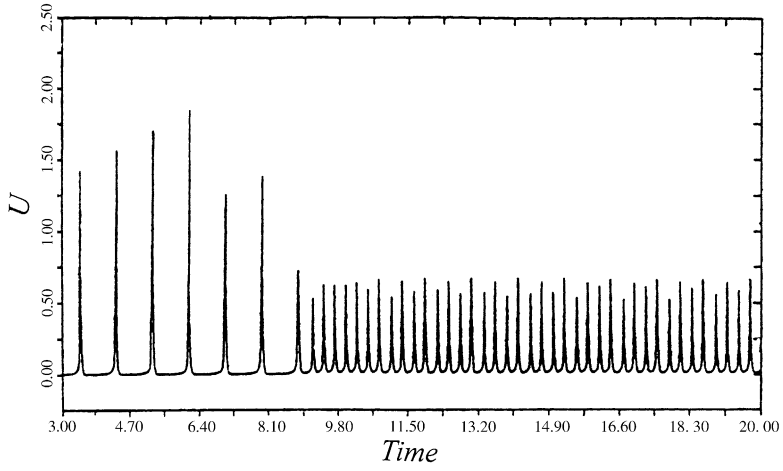

Fig. 5. Direct transition from Regimes II to IV. $P = 73.6333$ kPa, $T_0 = 565.15$ K, $\tau = 4$ s.

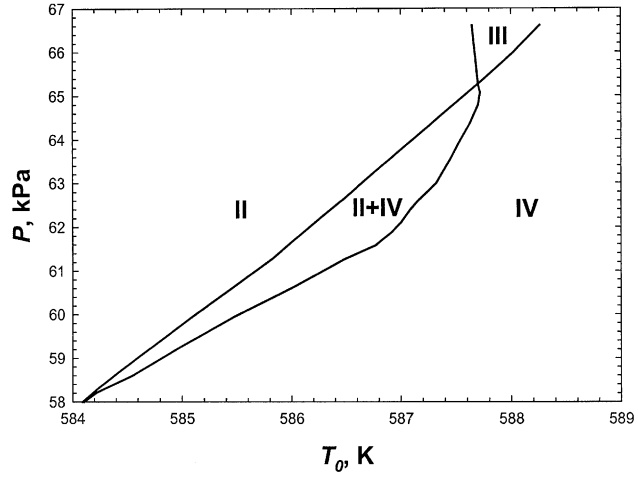

Fig. 6. Birhymicity regime predicted by Wang–Mou model. $\tau = 4$ s.

3.1.2. Bifurcations around regime (a)

Birhythmicity was noted in a narrow regime between points G and H, whose magnified phase diagram is displayed in Fig. 6. The width of this regime is approximately 0.5 K, while its temperature spans 4.5 K.

Cross-shaped topology is employed herein to interpret the birhythmic regime[15]. Fig. 6 presents a clear cross-shaped pattern, with Regimes II and IV positioned oppositely. While Regime III exhibits a mixed pattern of two-stage ignition (Regime II) and cool flame (Regime IV), while the birhythmic regime denotes a co-existence of two-stage ignition and cool flame. In Regime III the oscillation is controlled by folded slow manifold, and on each sheet the state is driven continuously and slowly. The oscillatory state is thus naturally unstable. Below point G in Fig. 1 the oscillatory state is stabilized on each sheet, and birhythmicity controls the process. The periods of cool flames along the boundary of Regimes II and III are fixed, which correlate with the experiments. Such a result excludes the occurrence of saddle point bifurcation on the boundary of Regimes II and III.

3.1.3. Bifurcations in regime (b)

According to Eq. (3), the steady-state heat generation and heat release rates can be stated as follows:

$$R(U) = k_T U = k_1 h_1 y_S + (k_2 h_2 y_S + k_3 h_3 + k_4 h_4 + k_5 h_5) x_S, \quad (5)$$

where x_s and y_s denote the corresponding steady-state solutions. Fig. 7 displays the functional values of $R(U)$. According to this illustration, the Wang–Mou model exhibits a maximum of three steady states, with the lowest being the stable focus, the middle one being the saddle point,

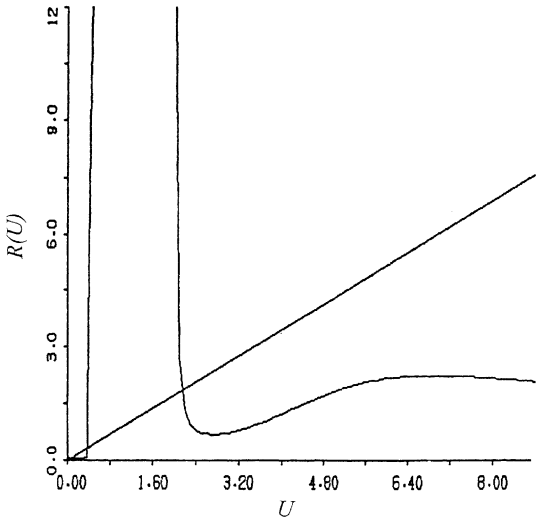

Fig. 7. Heat generation rate $R(U)$ and heat release rate $k_T U$ for Wang–Mou model. Three singularity points are noted. $P = 73.6333$ kPa, $T_0 = 590$ K, $\tau = 4$ s.

and the highest one denoting an unstable or stable focus. The basic dynamic characteristics of the Wang–Mou model thus differ from the Gary–Yang model, for which a maximum of four singularity points were identifiable (Gonda & Gray, 1983).

Figs. 8a–c present the bifurcation diagrams at $P =$ 374.7716, 335.322, and 44.1800 kPa, respectively, which represent horizontal lines crossing the bistable regimes in Fig. 1. The upper-branch solution moves downward as T_0 increases, corresponding to the negative temperature coefficient (NTC) regime. The stable steady states along the upper branch display stable focus dynamics, which correspond to Regime V (high-temperature steady states) in Fig. 1. Hopf bifurcation occurs along the upper branch at some T_0, where the stable focus becomes unstable. Since no hysteresis is noted, and the amplitude of oscillation is relatively small close to the bifurcation point, the bifurcation is recognized as a supercritical Hopf bifurcation (Gray & Jones, 1984). Crossing the Hopf bifurcation enters Regime IV where the cool flame occurs. The oscillation period increases gradually with decreasing T_0.

At $P = 49.9654$ kPa (Fig. 8a) the lower two steady-state branches form a continuous curve. As P decreases the upper branch approaches the middle solution. As Fig. 8b reveals, these two solutions had already merged at $P = 44.7059$ kPa. Restated, a fork bifurcation occurs at point D in Fig. 1. At $T_0 > T_0$(D), only one stable node exists. At point D, the fork bifurcation causes two stable nodes, while the upper branch adopts a stable focus. The bistable regime ranges from 596 to 620 K, corresponding to the regime BCDB (I+V) in Fig. 1. Meanwhile, at a still lower P the upper two solutions form a continuous curve (Fig. 8c). The regime BCDB is thus a cusp and point D represents a cusp bifurcation.

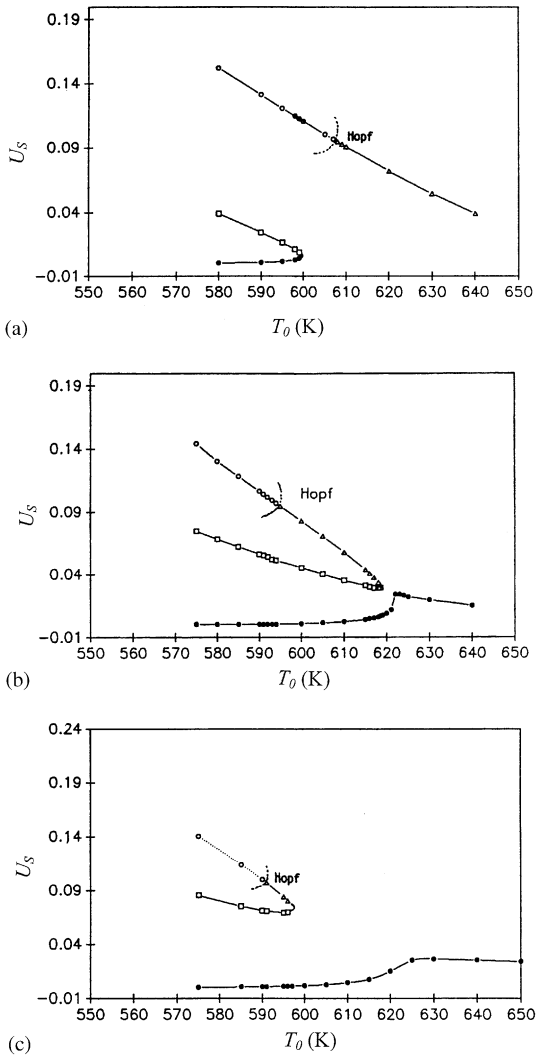

Fig. 8. (a) Bifurcation diagram at boundary of Regimes I and II. Open circle: unstable focus; open triangle: stable focus; close circle: stable node; open square: saddle point. $P = 49.9654$ kPa, $\tau = 4$ s. (b) Bifurcation diagram at boundary of Regimes I and II. Open circle: unstable focus; open triangle: stable focus; close circle: stable node; open square: saddle point. $P = 44.7059$ kPa, $\tau = 4$ s. (c) Bifurcation diagram at boundary of Regimes I and II. Open circle: unstable focus; open triangle: stable focus; close circle: stable node; open square: saddle point. $P = 44.1800$ kPa, $\tau = 4$ s.

In regime right to curve FBD in Fig. 1 contains neither a saddle point nor a stable focus. Curve FBD thus denotes the turning point of the lower two solutions at $P > P_D$, indicating the boundary of Regime I. Meanwhile, the turning point meets the Hopf bifurcation point at point B.

The upper and middle branches merge on curve DC in Fig. 1. In regime right to the curve DC in Fig. 1 contains only one stable mode, which correlates to the lower solution in Fig. 8c.

Regime ABCA indicates the bistable regime of I+IV. Reducing T_0 from curve ABC would create a larger limit cycle, which finally meets the stable manifold of the middle

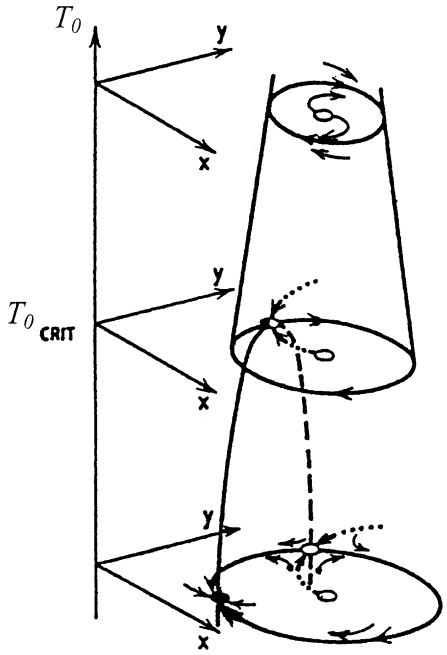

Fig. 9. The PNIPER bifurcation at the transition between Regimes I and II.

saddle point on curve AC. The state is then attracted to the lower steady state (Regime I). At a higher P, the upper steady state moves rightwards and upwards, as displayed in Fig. 8a. No bistable regime exists above point A in Fig. 1, due to the coincidence of the limit cycle and the saddle point on curve HA, which eliminates the unstable eigenvalues along the unstable manifold, while the remaining, stable eigenvalues still function.

The period of oscillation increases significantly (a jump) when the state moves toward curve FA from the right. Neither bistability nor hysteresis exist on the boundary among Regimes I and II, and the curve FA corresponds to the experimental findings conducted at large residence time (τ) (Gray et al., 1981a). The saddle-node infinite period bifurcation (SNIPER bifurcation) interprets the transition among Regimes I and II, and a limit cycle transits to the excitable state through SNIPER bifurcation (Noziticzins, Stirling, & Wittman, 1985; Noziticzins, Wittman, & Stirling, 1987; Gaspar & Galambosi, 1986).

Fig. 9 schematically illustrates the SNIPER bifurcation. The starting point is Regime II, where $T_0 > T_{0,\mathrm{CRIT}}$ given an unstable focus within the limit cycle. As the temperature decreases to $T_{0,\mathrm{CRIT}}$, saddle-node bifurcation occurs and breaks down the limit-cycle attractor to the low-temperature steady state (Regime I). An excitable steady state always exists, regardless of the direction of transition, from Regimes I to II, or vice versa. The prolonged oscillation period at II–I transition corresponds to the critical slowing phenomena when the limit cycle meets the unstable singularity close to the turning point (Dewel, 1985).

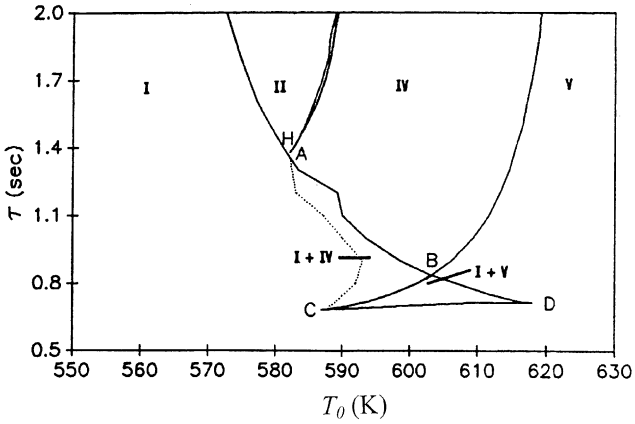

Fig. 10. The $\tau - T_0$ bifurcation diagram for acetaldehyde oxidation predicted by Wang–Mou model. $\tau = 4$ s.

3.2. $\tau - T_0$ diagram

Fig. 10 presents the bifurcation diagram on $\tau - T_0$ space at $P = 73.6333$ kPa. Five dynamic regimes similar to those in the $P - T_0$ diagram were also noted in the $\tau - T_0$ space. The corresponding bifurcations between Regimes I and II, II and III and IV and V correlate with those observed above.

According to Fig. 10, point B is located at $\tau = 0.84$ s and $T_0 = 604$ K; point D is located at $\tau = 0.717$ s and $T_0 = 617$ K; and point C is located at $\tau = 0.685$ s and $T_0 = 586.88$ K. Neither bistability nor hysteresis is detected for the transition from I to II, corresponding to the SNIPER bifurcation. The II–IV birhythmicity regime has a width of 0.6 K and a span of 7 K. Bistability occurs when τ ranges from 0.685 to 1.38 s.

3.3. Energy production rate and NTC regime

Experimental measurement of heat release rate is most restricted in Regimes I and V since these states are stationary. Meanwhile, the NTC regime correlates with the occurrence of cool flames. The present simulation results reveal that the Hopf bifurcation (cool flame) generally occurs along the NTC regime (the upper branch in Figs. 7a–c).

Average energy production is defined herein as follows:

$$\langle R \rangle = \int_a^b (k_2 h_2 y + k_3 h_3 + k_4 h_4) x \, \mathrm{d}t/(b-a). \tag{6}$$

In Regimes II–IV, where oscillations occur, a and b denote the starting time and ending time of a oscillation period, respectively. Regimes I and V only report the steady-state values. Fig. 11 displays the $\langle R \rangle$ values at $P = 73.6333$ kPa, with the dashed curves representing the oscillatory states, while the dot curves represent the stationary state. The steady-state solutions in Regimes II–IV are naturally unstable.

Only a low-temperature steady state exists in Regime I, where the most essential parameter is k_3. The heat production rate increases with T_0. Entering Regime II, due to the

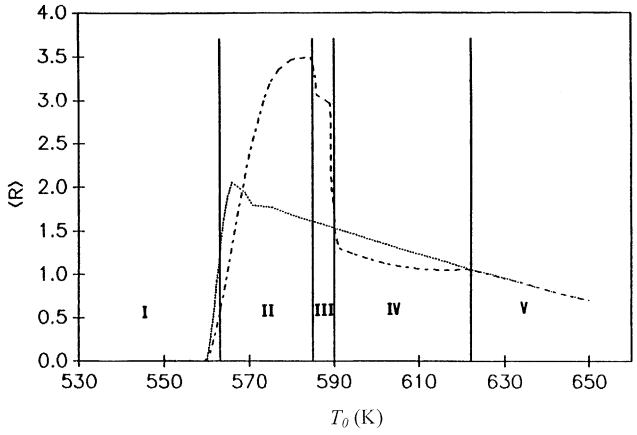

Fig. 11. Energy production rates for Regimes I–V. $P = 73.6333$ kPa, $\tau = 4$ s.

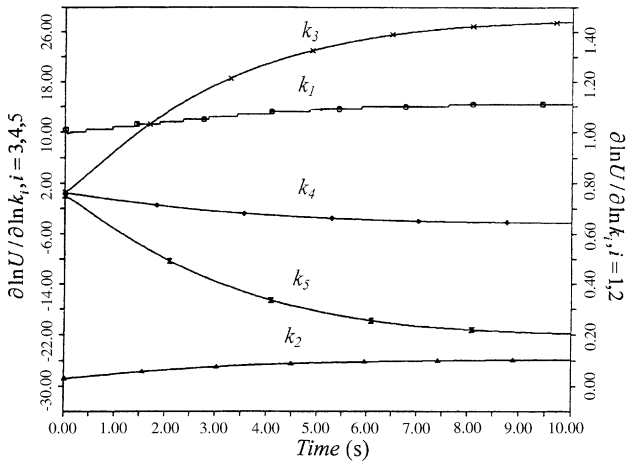

Fig. 12. The normalized SC, $\partial \ln x / \partial \ln k_i$, $i = 1$–5, $P = 73.6333$ kPa, $T_0 = 560$ K (Regime I), $\tau = 4$ s.

high-temperature branching mechanism, heat generation increases markedly with increasing T_0. The energy production rate reaches its maximum on the II–III boundary. In Regime III, the incorporation of cool flames during the complex oscillations on the contrary reduces heat generation at higher temperatures, corresponding to the NTC regime. Such an observation does not respond to previous studies and is attributed to the fact that although the high temperature termination step would release significant heat, the concentration of the branching agent declines, providing significant compensation for the effect of heat generation. In Regime IV, which is dominated by cool flames, the energy generation rate for the oscillatory state is even lower than that for the stationary state, and consequently the corresponding entropy production rate can be maintained at a low level to stabilize the system. Whether the system evolves according to the criterion of "minimum energy (entropy) production rate" remains unclear. In Regime V, U_s decreases with increasing T_0, thus reducing the energy production rate.

4. Sensitivity analysis

This section summarizes sensitivity analysis on the kinetic parameters of the Wang–Mou model performed herein to elucidate the dynamic behavior. Several methods can be adopted for the sensitivity analysis of parameters in a dynamic model, including Fourier amplitude sensitivity test (Cukier, Levine, & Schuler, 1978), direct method (Atherton, Schaniker, & Ducot, 1975; Dickinson & Gelinas, 1976), Green's function method (Dougherty, Hwang, & Rabitz, 1979; Hwang, Dougherty, Rabitz, & Rlitz, 1978), and polynomial approximation method (Hwang, 1983, 1985). PAM requires a relatively short computational time and small storage memory, and the related programming is very simple. The sensitivity analysis was conducted for the Wang–Mou model using PAM.

In PAM the governing equations (Eqs. (4a)–(4c)) are first solved numerically, and the whole integration interval is then divided into numerous subintervals. A third- or forth-order interpolation polynomial (such as Lagrange, Legendre, or the Jacobi polynomial) is employed in each subinterval to represent the dynamical response, and the system parameters are then expanded using expansion coefficients, which transform the original sensitivity analysis equations into algebraic equations for solution.

The analysis is focuses on the sensitivity of reaction species and temperature to kinetic parameter k_i. The parameters are set as $P = 73.6333$ kPa and $\tau = 4$ s.

4.1. Regime I

Fig. 12 displays the PAM results at $T_0 = 560$ K (Regime I), and Tables 2 and 3 summarize the calculation results. Since the corresponding steady state is a stable node, x and U increase over time while y remains almost constant. The sensitivity coefficient (SC) data reveal that the change in x and U with respect to k_i ($i = 1$–5) become invariant after $t = 9$ s, while that of y is independent of time throughout the entire integration domain.

In accordance with the normalized SCs shown in Fig. 12, k_1 is the most important parameter at the start of the reaction. The significance of k_3 and k_5 increases over time; while the effects of k_2 and k_4 are generally negligible. The following thermokinetic interpretations are made. Initiation reaction (Eq. (2a)) occurs first and generates x slowly due to the high activation energy of E_1. Since the change in y is negligible, k_2 remains insignificant. After x has been accumulated a substantial amount the subsequent reactions, the low-temperature branching (Eq. (2c)) and the low-temperature termination (Eq. (2e)), occur rapidly to reach a steady state. The final steady state is determined by the competition between the branching and termination steps, whose significance is $k_3 > k_5$. Consequently the SC

Table 2
Normalized sensitivity coefficients at low-temperature steady state (560 K, Regime I) and high-temperature steady state (640 K, Regime V)

	$\partial \ln x/\partial \ln k_1$	$\partial \ln x/\partial \ln k_2$	$\partial \ln x/\partial \ln k_3$	$\partial \ln x/\partial \ln k_4$	$\partial \ln x/\partial \ln k_5$
560 K	1.11	0.0718	26.9	−4.65	−21.7
640 K	0.0242	−0.168	0.243	−0.965	−0.102
	$\partial \ln y/\partial \ln k_1$	$\partial \ln y/\partial \ln k_2$	$\partial \ln y/\partial \ln k_3$	$\partial \ln y/\partial \ln k_4$	$\partial \ln y/\partial \ln k_5$
560 K	0	0	0	0	0
640 K	−0.0392	−0.0398	−0.316	0.267	0.0812
	$\partial \ln U/\partial \ln k_1$	$\partial \ln U/\partial \ln k_2$	$\partial \ln U/\partial \ln k_3$	$\partial \ln U/\partial \ln k_4$	$\partial \ln U/\partial \ln k_5$
560 K	1.11	0.103	27.6	−4.22	−21.8
640 K	0.226	0.288	4.62	−3.64	−1.18

Table 3
Normalized sensitivity coefficients at low-temperature steady state (560 K, Regime I) and high-temperature steady state (640 K, Regime V)

	Sxh_2/Sxh_3	Sxh_2/Sxh_4	Sxh_3/Sxh_4
560 K	0.0589	0.0675	1.147
640 K	1.268	0.305	0.241
	Syh_2/Syh_3	SyH_2/SyH_4	Syh_3/Syh_4
560 K	0.0589	0.0675	1.146
640 K	1.26	0.304	0.242
	SUh_2/SUh_3	SUH_2/SUH_4	SUh_3/SUh_4
560 K	0.0589	0.0675	1.146
640 K	1.265	0.305	0.241
	Sxxo/Sxyo	Sxxo/SxUo	Sxyo/SxUo
560 K	824	618	0.75
640 K	0/0	0/0	0/0
	Syxo/Syyo	Syxo/SyUo	Syyo/SyUo
560 K	0/0	0/0	0/0
640 K	0/0	0/0	0/0
	SUxo/SUyo	SUxo/SUUo	SUyo/SUUo
560 K	824	618	0.75
640 K	0/0	0/0	0/0

sequence follows the pattern $k_3 > k_5 > k_4 > k_1 \gg k_2$ in Regime I, where high-temperature reactions are unimportant.

4.2. Regime V

Figs. 13 and 14 illustrate the SC at high temperature ($T_0 =$ 640 K), and Tables 2 and 3 also summarize the calculation results. As Fig. 13 reveals, x and U evolve rather fast, and the reaction stabilizes (stable focus) within 3 s. The normalized SC for y are not zero, indicating increasing importance

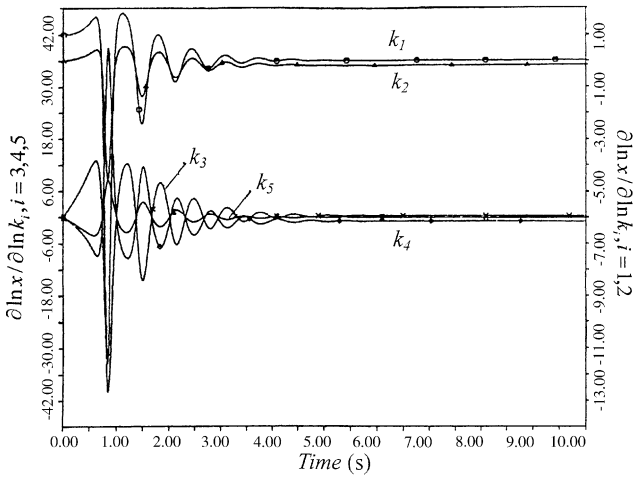

Fig. 13. The normalized SC, $\partial \ln x/\partial \ln k_i$, $i = 1$–5, $P = 73.6333$ kPa, $T_0 = 640$ K (Regime V), $\tau = 4$ s.

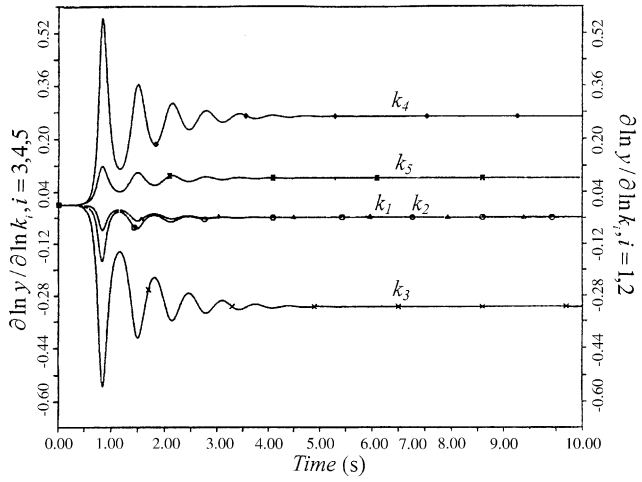

Fig. 14. The normalized SC, $\partial \ln U/\partial \ln k_i$, $i = 1$–5, $P = 73.6333$ kPa, $T_0 = 640$ K (Regime V), $\tau = 4$ s.

of k_2. Although the normalized SC for x and U with respect to k_i are less than at 560 K, the sequence of significance can still be identified as follows: $k_3 > k_4 > k_5 > k_2 > k_1$.

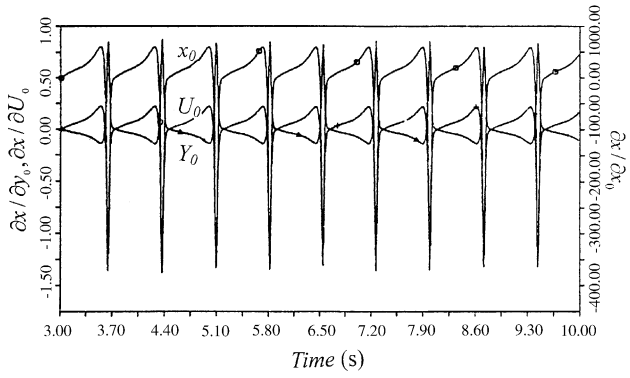

Fig. 15. (a) The normalized SC for evolutions of x respect to initial conditions. $P = 73.6333$ kPa, $T_0 = 600$ K (Regime IV), $\tau = 4$ s. (b) The normalized SC for evolutions of x respect to initial conditions. $P = 73.6333$ kPa, $T_0 = 620$ K (Regime IV), $\tau = 4$ s.

Apparently the significance of thermal branching (k_2) and high-temperature termination (k_4) increases substantially in Regime V compared to Regime I.

As Table 3 lists, the normalized SC for x, y and U with respect to h_3 is the most significant parameter at 560 K, while at 640 K, h_2 becomes the most significant parameter. h_i mainly influences the variable U. Consequently, U is mainly controlled by k_3 in low-temperature regimes. As temperature rises, the controlling parameter becomes k_2, and thus the low-temperature branching was activated at 560 K, while the high-temperature branching controls the dynamics at 640 K.

4.3. Regime IV

Edelson (1981a, b), Larter (1983), and Larter, Rabitz, and Kramer (1984) conducted sensitivity analysis on the limit-cycle attractor of BZ reactions, and defined a quantity called period sensitivity coefficient as follows:

$$\frac{\partial \tau}{\partial \alpha_k} = \frac{\partial t}{\partial C_i}\left\{\left(\frac{\partial C_i}{\partial \alpha_k}\right)_t - \left(\frac{\partial C_i}{\partial \alpha_k}\right)_{t+\tau}\right\}, \tag{7}$$

where α_k denotes the initial conditions (x_0, y_0 and U_0 herein), C_i represents the variables involved (x, y and U), and τ, is the period. If the attractor being investigated is a stable limit cycle, the period sensitivity coefficient is zero regardless of the initial condition α_k, reflecting that the period of a limit cycle is unaffected by the initial conditions.

Figs. 15a and b illustrate that, during $T_0 = 600$–620 K, both $\partial x/\partial \alpha_k$ and $\partial U/\partial \alpha_k$ oscillate periodically. Inasmuch as the corresponding $\partial \tau/\partial \alpha_0$'s are null, the cool flames are a stable limit-cycle attractor.

Reducing T_0 to 595 K, which is close to the III–IV boundary in Fig. 1, the corresponding $\partial \tau/\partial \alpha_k$ would no longer be zero (data not shown). Similar results are also noted at 622 K (data not shown), which is close to the IV–V boundary. The limit-cycle attractor thus gradually destabilizes when approaching the Hopf bifurcation point.

Table 4 lists the average $\partial \tau/\partial \alpha_0$ over 10 periods of oscillations at $T_0 = 600$ and 605 K. The significance of k_i on the period of limit cycle follows the pattern: $k_1 \gg k_2 > k_3 > k_5 > k_4$. Consequently, the rate constant k_1 controls the period of cool flame. This occurrence is attributed to x initially being slowly formed through Eq. (2a), whose formation spends a long period of time (high activation energy E_1). Following the initiation stage the subsequent reactions (Eqs. (2c)–(2e)) proceed rapidly. Consequently, the controlling step for the cool flame period is the initiation step (Eq. (2a)).

Table 4
Sensitivity coefficients in cold-flame regime (Regime IV)

600 K				
$\partial\tau/\partial k_1$	$\partial\tau/\partial k_2$	$\partial\tau/\partial k_3$	$\partial\tau/\partial k_4$	$\partial\tau/\partial k_5$
−218.0	−2.628	−1.401	1.325	1.0
−224.1	−2.327	−1.401	1.335	1.0
−217.7	−2.613	−1.396	1.330	1.0
−212.4	−2.554	−1.380	1.318	1.0
−234.9	−2.760	−1.436	1.375	1.0
−216.4	−2.640	−1.400	1.332	1.0
−220.6 (ave)	−2.588 (ave)	−1.402 (ave)	1.336 (ave)	1.0 (ave)
605 K				
$\partial\tau/\partial k_1$	$\partial\tau/\partial k_2$	$\partial\tau/\partial k_3$	$\partial\tau/\partial k_4$	$\partial\tau/\partial k_5$
−187.5	−2.414	−1.273	1.242	1.0
−207.8	−2.355	−1.333	1.280	1.0
−203.2	−2.419	−1.352	1.286	1.0
−207.0	−2.304	−1.310	1.266	1.0
−208.6	−2.353	−1.325	1.270	1.0
−198.8	−2.272	−1.281	1.218	1.0
−202.1 (ave)	−2.353 (ave)	−1.309 (ave)	1.260 (ave)	1.0 (ave)

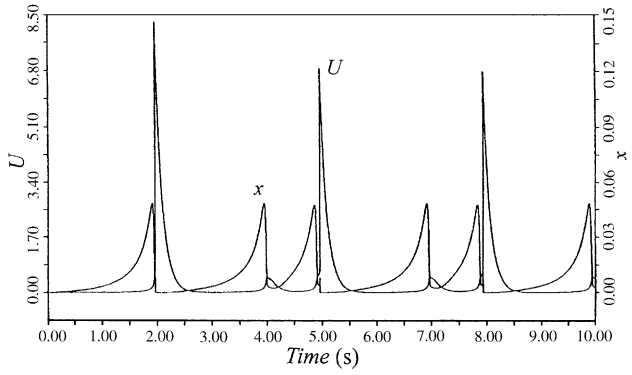

Fig. 16. Time evolutions of x and U at state P_1^1 in Regime III. $P = 73.6333$ kPa, $T_0 = 587$ K, $\tau = 4$ s.

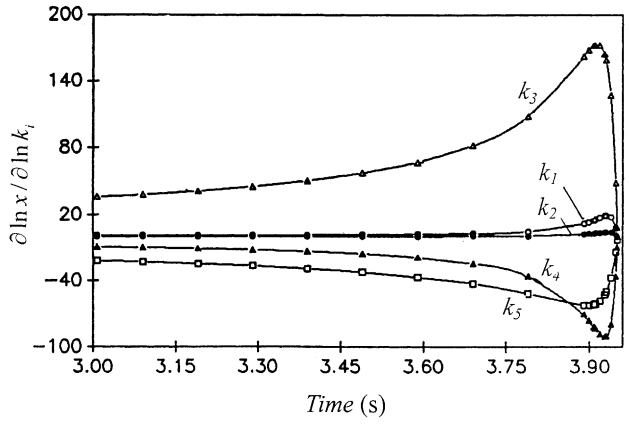

Fig. 17. The normalized SC, $\partial \ln x/\partial \ln k_i$, $i = 1$–5, $P = 73.6333$ kPa, $T_0 = 587$ K (cool flame at P_1^1 state in Regime I), $\tau = 4$ s.

4.4. Regimes II and III

Regime II contains only cool flames, while Regime III presents a mixed mode of cool flame and two-stage ignition. Once a cool flame or a two-stage ignition occurs, they share similar SCs. Consequently, only the P_1^1 state in Regime III (which occurred at 587 K) is used herein as an illustrative example.

Fig. 16 illustrates the time evolutions of U and x. During each period of P_1^1 one cool flame and one two-stage ignition exist. A cool flame initiated at $t = 1.92$ s. Fig. 17 present the normalized SC during the occurrence of the cool flame. The $\partial \ln x/\partial \ln k_i$'s ($i = 1$–3) are positive; while the remaining two are negative. The normalized SC changed signs when species x maximized (x_{max}) at $t = 3.95$ s. Restated, $\partial \ln x/\partial \ln k_i$ ($i = 1$–3) become negative; while the remainder remain positive. At $t = 4.12$ s, the state resumes its initial condition. The cool flame completes its oscillation during 1.92–4.12 s.

Starting from $x = x_{min}$, the rate constants follow the following sequence of significance. At x_{min}, $k_4 > k_3 > k_1 > k_5 > k_2$. Meanwhile, when x is greater (but still below x_{max}) the absolute values of SCs reach their peak, and the sequence becomes $k_3 > k_4 > k_5 > k_1 > k_2$. At $x = x_{max}$, the sequence is $k_3 > k_4 > k_1 > k_5 > k_2$. Meanwhile, the absolute values of SCs reached their minimum with a further increase in x. The corresponding sequence is $k_4 > k_1 > k_3 > k_2 > k_5$, and the sequence restores its initial consequence at x_{min}, $k_4 > k_3 > k_1 > k_5 > k_2$. Table 5 summarizes some numerical results.

The cool flame is followed by two-step ignition. The duration of 4.12–4.93 s corresponds to the cool-flame precursor for the two-stage ignition, while the changes in SCs are identical to those presented in Fig. 17. The concentration of x increases during 4.12–4.86 s, and the SCs for x with respect to k_i, $i = 1$–3, are positive, while those for $i = 4$ and 5 are negative. x_{max} occurs at $t = 4.86$ s, where the SCs change their signs. At $t = 4.93$ s the state reaches $x = x_{min}$, signaling the end of cool flame precursor. Meanwhile, the thermal ignition stage begins at $t = 4.93873$ s. x reaches a second, small x_{max} at 4.95 s. Finally, at $t = 4.96746$ s both x and y are completely exhausted and the cycle is completed.

Table 5 summarizes some computed SCs. During the thermal ignition stage the most influential parameter is k_1. Within a brief period (4.95873–4.96746 s), following slightly behind the occurrence of x_{max}, SCs change signs twice with amplitudes of up to 10^5–10^{11}. This observation closely corresponds to the peak temperature. The above-mentioned oscillatory pattern repeats itself in P_1^1, while the SCs, $\partial \ln x/\partial \ln k_i$, during thermal ignition follow the sequence: $k_1 > k_2 > k_4 > k_3 > k_5$.

The SCs for the (simple) two-stage ignition stage observed in Regime II are also numerically evaluated. The full cycle correlates with that noted in the two-stage ignition stage in Regime III.

5. Concluding remarks

The dynamic behavior of the Wang–Mou model is explored in detail herein using numerical simulations. The investigated parametric range is wider than that in Wang and Mou (1985). Three singularity points were identified in the Wang–Mou model. Five distinct dynamic regimes reported in the literature were noted: (I) low-temperature steady state (stable node), (II) oscillatory two-stage ignitions, (III) complex oscillations (IV) oscillatory cool flames, and (V) high-temperature steady state (stable focus) on the $P - T_0$ and $\tau - T_0$ diagrams. With the denotation of P_1^m, as in the case with one large-amplitude oscillation and m small-amplitude oscillations during a period, the bifurcation in Regime III presents an odd-m sequence ($m = 1, 3, 5, \ldots$) or an even-m ($m = 2, 4, 6, \ldots$) sequence. Between the P_1^m and P_1^{m+2} states "windows" of chaos exist. At large and small P (or τ) limits Regime III vanishes when direct transition between Regimes II and IV is possible.

Besides the above five regimes, a regime of birhythmicity and two bistable regimes (I+IV and I+V) were also noted. Cross-shapes topology interpreted the birhythmicity regime

Table 5
Sensitivity coefficients for complex oscillation P_1^1 (Regime III). $T_0 = 587$ K

Time (s)	$\partial \ln x/\partial \ln k_1$	$\partial \ln x/\partial \ln k_2$	$\partial \ln x/\partial \ln k_3$	$\partial \ln x/\partial \ln k_4$	$\partial \ln x/\partial \ln k_5$
3.00000	1.27	0.199	36.0	−9.04	−21.4
3.29000	1.49	0.253	45.3	−11.7	−26.4
3.59000	2.36	0.445	66.8	−18.7	−36.4
3.89000	12.4	2.71	162	−70.4	−62.5
3.89873	13.9	3.05	168	−75.9	−62.4
3.90946	156	3.44	172	−81.6	−61.4
3.91000	16.1	3.56	172	−83.2	−60.9
3.91873	17.9	4.00	172	−88.3	−58.0
3.92746	19.5	4.36	164	−90.4	−52.3
3.93000	19.7	4.44	159	−89.7	−49.8
3.93873	18.5	4.17	127	−79.4	−37.3
3.94746	8.23	1.74	49.0	−35.7	−13.2
3.95000	0.89	−0.013	9.25	−9.02	−2.55
3.95873	−64.7	−15.9	−273	193	54.6
3.96746	−359	−89.1	−911	917	179
3.97000	−555	−139	−1230	1340	229
3.97873	−3310	−851	−4220	6170	624
3.98746	−17000	−4530	−11500	23500	1310
3.99000	−23200	−6250	−13500	30000	1430
3.99873	−32700	−8960	−14000	36800	1320
4.00746	−4500	−1240	−1830	4950	169
4.01000	−3200	−888	−1310	3520	121
4.86746	−4.61	−1.64	−18.6	9.71	4.53
4.87000	−24.1	−7.34	−106	72.1	25.8
4.87873	−208	−61.9	−681	570	145
4.88746	−1100	−335	−2330	2480	413
4.89000	−1800	−551	−3250	3760	540
4.89773	−11000	−3500	−10500	17100	1340
4.90746	−49400	−16300	−25200	57400	2490
4.91000	−55700	−18500	−25100	61000	2360
4.91873	−31900	−10700	−11600	31600	991
4.92746	−3220	−1120	−1040	2960	85.1
4.93000	−923	−354	−282	771	22.6
4.93873	3570	1140	1020	−3300	−78.5
4.94746	11200	3640	2590	−9340	−183
4.95000	88600	29200	18800	−70900	−1280
4.95873	-4.09×10^5	-1.40×10^5	-4.80×10^4	2.48×10^5	2570
4.96746	2.54×10^{11}	1.29×10^{11}	3.45×10^7	-6.29×10^9	-1.14×10^5
4.97000	1.90×10^9	9.64×10^9	2.68×10^5	-4.86×10^7	−899
4.97873	2.27×10^8	1.16×10^8	3.64×10^4	-6.15×10^7	−129
4.98746	1.35×10^9	6.74×10^9	2.48×10^5	-3.91×10^7	−932
4.99000	5.75×10^8	2.87×10^8	1.10×10^5	-1.77×10^7	−420
4.99873	4.85×10^8	2.40×10^8	1.08×10^5	-1.54×10^7	−436
5.00746	4.41×10^8	2.03×10^8	1.07×10^5	-1.41×10^7	−462
5.01000	3.90×10^8	1.91×10^8	1.06×10^5	-1.36×10^7	−465

as the co-existence of two-stage ignitions and cool flames, which was found in a narrow regime beside the intersection point of Regimes II, III and IV. The transition between Regimes I and II in the bistable regime reveals a saddle-node infinite period bifurcation (SNIPER bifurcation). Furthermore, the periods of cool flames along the boundary of Regimes II and III are fixed, which excludes the occurrence of saddle point bifurcation on the boundary.

Sensitivity analysis using the PAM reveals that in Regime I, where the high-temperature reactions are unimportant, the SC of the five kinetic parameters follow the pattern: $k_3 > k_5 > k_4 > k_1 \gg k_2$. Meanwhile, in Regime V the sequence is $k_3 > k_4 > k_5 > k_2 > k_1$. The significance of thermal branching (k_2) and high-temperature termination (k_4) increases substantially in Regime V compared with in Regime I.

In Regime IV (cool-flame regime) the significance of k_i on the period of the limit cycle follows the pattern: $k_1 \gg k_2 > k_3 > k_5 > k_4$. The rate constant k_1 thus controls the period of cool flame, mainly because of its relatively high activation energy E_1. Moreover, $k_3 > k_5 > k_4 > k_1 > k_2$ in the x-increasing phase, and $k_4 > k_3 > k_1 > k_5 > k_2$ in the x-decreasing phase, respectively. The ignition oscillation occurs after the cool flame in Regimes II and III, this oscillation exhibits a two-step ignition characteristic. In the cool-flame precursor, the changes in SCs are the same as in Regime IV, while during the ignition oscillation stage the SC follows the sequence $k_1 > k_2 > k_4 > k_3 > k_5$.

Acknowledgements

The authors are grateful to National Science Council, ROC for financial support.

References

Atherton, R. W., Schaniker, R. B., & Ducot, E. R. (1975). On the statistical sensitivity analysis of models for chemical kinetics. *A.I.Ch.E. Journal*, *21*, 441–448.

Cavangh, J., Cox, R. A., & Olson, G. (1990). Computer modeling of cool flames and ignition of acetaldehyde. *Combustion and Flame*, *82*, 15–39.

Cukier, R. I., Levine, H. B., & Schuler, K. E. (1978). Nonlinear sensitivity analysis of multiparameter model system. *Journal of Computational Physics*, *26*, 1–42.

Dewel, G. (1985). Relaxation kinetics and critical point behavior. *Journal of Physical Chemistry*, *89*, 4670–4672.

Dickinson, R. P., & Gelinas, R. J. (1976). Sensitivity analysis of ordinary differential equation systems—a direct method. *Journal of Computational Physics*, *21*, 123–143.

Di Maio, F. P., Lignola, P. G., & Talarico, P. (1993). Thermokinetic oscillation in acetaldehyde CSTR combustion. *Combustion Science and Technology*, *91*, 119–142.

Dougherty, E.P., Hwang, J.T., & Rabitz, H. (1979). Further developments and applications of the Green's function method of sensitivity analysis in chemical kinetics. *Journal of Chemical Physics*, *71*, 1974–1804.

Edelson, D. (1981a). Sensitivity analysis of oscillating reactions. 1. The period of the Oregonator. *Journal of Physical Chemistry*, *85*, 1555–1558.

Edelson, D. (1981b). Mechanistic details of the Belousov–Zhabotinsky oscillations. IV. Sensitivity analysis. *International Journal of Chemical Kinetics*, *13*, 1175–1190.

Felton, P. G., Gray, B. F., & Shank, N. (1976). Low temperature oxidation in a stirred flow reactor. *Combustion and Flame*, *27*, 363–376.

Gaspar, V., & Galambosi, P. (1986). Bifurcation diagram of the oscillatory Belousov-Zhabotinski system of oxalic acid in a continuous flow stirred-tank reactor. Further possible evidence of saddle node infinite period bifurcation behaviour of the system. *Journal of Physical Chemistry*, *90*, 2222–2226.

Gaspard, P., & Wang, X. (1987). Homoclinic orbits and mixed-mode oscillations in far-from equilibrium systems. *Journal of Statistical Physics*, *48*, 151–199.

Gibson, C., Gray, B. F., Griffiths, J. F., & Hasko, S. M. (1984). *Twentieth symposium on combustion*, The Combustion Institute.

Gonda, I., & Gray, B. F. (1983). The unified thermal and chain branching model of hydrocarbon oxidation in a well stirred continuous flow reactor. *Proceedings of Royal Society of London*, *series A*, Vol. 389 (pp. 133–152).

Gray, P., Griffiths, J. F., Hasko, S. M., & Lignola, P. G. (1981a). Oscillatory ignitions and cool flames accompanying the non-isothermal oxidation of acetaldehyde in a well stirred, flow reactor. *Proceedings of Royal Society of London*, *series A*, 374 (pp. 313–339).

Gray, P., Griffiths, J. F., Hasko, S. M., & Lignola, P. G. (1981b). Novel, multiple-stage ignitions in the spontaneous combustion of acetaldehyde. *Combustion and Flame*, *43*, 175–186.

Gray, B. F., & Jones, J. C. (1984). The heat release rate and cool flames of acetaldehyde oxidation in a continuously stirred tank reactor. *Combustion and Flame*, *57*, 3–14.

Griffiths, J. F. (1995). Reduced kinetic-models and their application to practical combustion systems. *Progress in Energy and Combustion Science*, *21*, 25–107.

Griffiths, J. F., & Sykes, A. F. (1989). Numerical studies of a thermokinetic model for oscillatory cool flame and complex ignition phenomena in ethanl oxidation under well-stirred flowing conditions. *Proceedings of Royal Society of London*, *series A*, Vol. 422 (pp. 289–310).

Halstead, M. P., Prothero, A., & Ouinn, C. P. (1971). A mathematical model of the cool-flame oxidation of acetaldehyde. *Proceedings of Royal Society of London*, *series A*, Vol. 322 (pp. 377–403).

Harrison, A. J., & Cairnie, L. R. (1988). The development and experimental validation of a mathematical model for predicting hot-surface auto-ignition hazards using complex chemistry. *Combustion and Flame*, *71*, 1–21.

Hwang, J. T. (1983). Sensitivity analysis in chemical kinetics by the method of polynomial approximations. *International Journal of Chemical Kinetics*, *15*, 959–988.

Hwang, J. T. (1985). A computational algorithm for the polynomial approximation method of sensitivity analysis in chemical kinetics. *Journal of Chinese Chemical Society*, *32*, 253–261.

Hwang, J. T., Dougherty, E. P., Rabitz, S., & Rlitz, H. (1978). The Green's function method of sensitivity analysis in chemical kinetics. *Journal of Chemical Physics*, *69*, 5180–5191.

Kaiser, F. W., Westbrook, C. K., & Pitz, W. J. (1986). Acetaldehyde oxidation in the negative temperature coefficient. *International Journal of Chemical Kinetics*, *18*, 655–688.

Larter, R. (1983). Sensitivity analysis of autonomous oscillations. Separation of secular terms and determination of structural stability. *Journal of Physical Chemistry*, *87*, 3114–3121.

Larter, R., Rabitz, H., & Kramer, M. (1984). Sensitivity analysis of limit cycles with application to the Brusselator. *Journal of Chemical Physics*, *80*, 4120–4128.

Nosziticzins, Z., Stirling, P., & Wittman, M. (1985). Measurement of bromine removal rate in the oscillatory BZ reaction of oxalic acid. Transition from limit cycle oscillations to excitability via saddle-node infinite period bifurcation. *Journal of Physical Chemistry*, *89*, 4914–4921.

Nosziticzins, Z., Wittman, M., & Stirling, P. (1987). Bifurcation from excitability to limit cycle oscillation at the end of the induction period in the classical Belousov–Zhabotinsky reaction. *Journal of Chemical Physics*, *86*, 1922–1926.

Pugh, S. A., De Kock, B., & Ross, J. (1986). Effects of two periodic perturbations on the oscillatory combustion of acetaldehyde. *Journal of Chemical Physics*, *85*, 879–886.

Scott, S. K. (1991). *Chemical chaos*. London: Oxford University Press.

Wang, X., & Gaspard, P. (1990). In P. Gray, N. Nicolis, F. Baras, P. Borckmans, & S. K. Scott (Eds.), In *Spatial inhomogeneities and transient behaviour in chemical kinetics*. Manchester: Manchester University Press.

Wang, X., & Mou, C. Y. (1985). A thermokinetic model of complex oscillations in gaseous hydrocarbon oxidation. *Journal of Chemical Physics*, *83*, 4554–4561.

Yang, C. H., & Gray, B. F. (1969). On the slow oxidation of hydrocarbon and cool flames. *Journal of Physical Chemistry*, *73*, 3395–3406.